Universiteit Utrecht

Opleiding Natuur- en Sterrenkunde

Testing general relativity: Event Horizon Telescope versus LIGO/Virgo

Bachelor Thesis

Louis M.H. Verhees

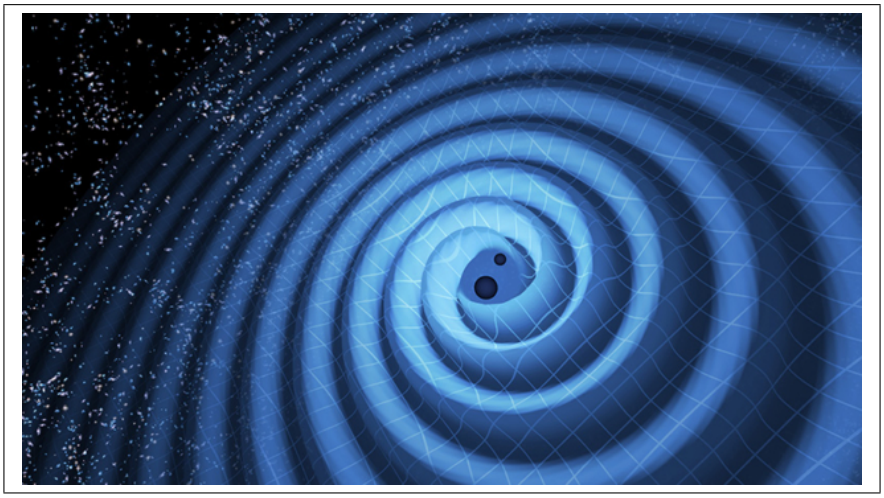

Taken from [4]

Supervisor:

Prof. Dr. C.F.F. Van Den Broeck
Utrecht University, Institute for Gravitational and Subatomic Physics

June 15, 2021

Abstract

Recently the black hole nature of the compact object imaged by Event Horizon Telescope (EHT) was tested by putting bounds on a possible $1/r^3$ correction to the Newtonian potential. Here we perform a similar test, but using the gravitational wave (GW) signals from binary black hole inspirals. First we calculate how the phasing of a GW signal changes when introducing the same modification to the potential as with EHT. Next we select two gravitational wave detections from binary black holes, GW151226 and GW170608, whose long inspirals are particularly suited for the test at hand. Finally, we use publicly available LIGO-Virgo data to bound the dimensionless coefficient associated with the modification of the potential. The bounds we obtain this way are found to be similar to those of EHT.

Contents

1 Introduction

The theory of general relativity (GR) developed by Albert Einstein [17] was introduced in 1916 and has been massively impacted our understanding on the nature of the universe. The theory where space and time become one and where masses can bend space-time has been tested over the last 100 years, where the first test was performed in 1919 during a total solar eclipse. It has been proved by a large number of experiments up to this day. Recently we have reached a new milestone in confirming the legitimacy of GR by the detection of gravitational waves (GW's). Over 100 years ago Einstein already stated that these GW's could exist purely on a theoretical basis. And since 1974 we have indirect measurements of these GW's [20]. In 2015 the first detection was made by a detector in the united states called LIGO and until this day we have over 50 detections coming from multiple detectors all over the world.

But in the era of modern physics there also arose a very different theory which focuses on the smallest length scale: quantum mechanics (QM). With these two theories we are capable of describing nature from the smallest atomic scale to the scale of the universe, but they are in no way compatible with each other. This is the reason why many physicist believe that QM nor GR tells the whole story and this encourages us to explore the edge of our understanding of gravity and to test GR. A good way to do this is by studying black holes. This is done by using radio interferometry (the Event horizon telescope) to optically measure a black hole and by studying gravitational waves coming from either binary black holes or binary neutron stars.

In this thesis we will test GR by using gravitational waves and we will compare them with the tests made by the event horizon telescope (EHT). By using measurements of GW's from LIGO and Virgo detectors we can set bounds on certain parameters that are defined by fundamental physics. We do this by using the post-Newtonian formalism. With this formalism we can approximate GR and study it in the weak field regime which is applicable to black hole binaries.

First we start of with briefly discussing the event horizon telescope and how it was able to take measurements of a black hole in chapter 2. Then in chapter 3 we will discuss what gravitational waves are and how we can detect them, after which we will focus on binary systems in chapter 4. In chapter 5 the binary inspiral will be discussed with a modified gravitational potential and the post-Newtonian formalism will be featured so we can define the parameter that we are interested in to eventually test GR in chapter 6 were we also discuss the data analysis necessary to extract the useful information. In the end we will set some concluding remarks and discuss our results.

2 The Event Horizon telescope

In this section we discuss the contributions of the event horizon telescope to tests of general relativity. The Event Horizon Telescope is a network of telescopes all around the globe, which makes it possible to get pictures with a resolution far beyond the reach of any existing single telescope today. This so called radio-interferometer which can be virtually seen as a telescope the size of the earth, was able to get a picture of the 'shadow' of a supermassive black hole in the centre of the galaxy Messier 87 (M87) [9].

2.1 The shadow of a black hole

Using Event Horizon Telescope (EHT), a picture has been made of the "shadow" of a black hole. The outline of a black-hole shadow is the locus of the photon trajectories on the screen of a distant observer that, when traced backwards, become tangent to the surfaces of spherical photon orbits hovering just above the black-hole horizons [24].

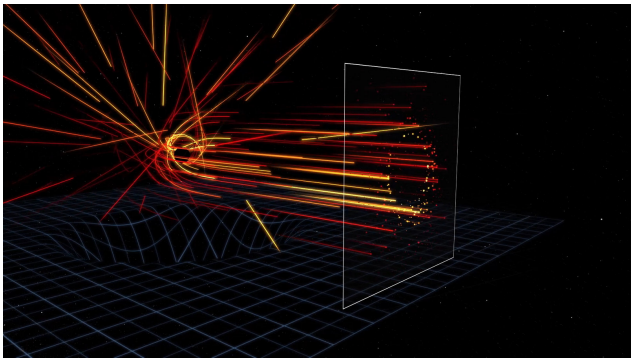

Figure 1: Photon trajectories that make up the shadow of the black hole. taken from [3]

2.2 The size of the shadow

From the picture of the black hole shadow we can determine the angle θ of the shadow. From astronomical data we know that the distance D to M87 is 15.4± 0.6Mpc [28] and from that we can calculate the radius of the shadow:

$$R_{sh} = Dtan(\theta) \tag{1}$$

From the movement of the surrounding matter of a black hole we can calculate the mass of the black hole. The mass of the black hole [18] gives us an theoretical radius of the shadow [23]:

$$r_{sh} = \frac{3\sqrt{3}GM}{c^2} \tag{2}$$

which comes from the theory of general relativity (GR). Now we want to compare this with the measured size of the shadow from the picture.

Figure 2: Picture of the black hole in the centre of M87. taken from EHT collaboration [10]

To do this we first explore analytically the shadow size for a general static, spherically symmetric space-time metric. Static because the size of the black hole shadow depends very weakly on the black hole spin so we can ignore that factor here. That leaves us with the following equation for the metric [24]:

$$ds^2 = g_{tt}dt^2 + g_{rr}dr^2 + r^2 d\Omega \tag{3}$$

According to GR the tt element is defined as

$$-g_{tt} = 1 - \frac{2GM}{rc^2} \tag{4}$$

For the shadow radius we have:

$$r_{sh} = \frac{r_{ph}}{\sqrt{-g_{tt}(r_{ph})}} \tag{5}$$

with r_{ph} defined as,

$$r_{ph} = \sqrt{-g_{tt}} \left(\frac{d\sqrt{-g_{tt}}}{dr}\Big|_{r_{ph}} \right)^{-1} \tag{6}$$

This gets us to Eq. (2), but from the picture (see figure 2) we can see that we definitely don't have an infinitely large resolution for the telescope so our picture is somewhat blurry. This results in an uncertainty for the measurement of the shadow radius. We can assign a certain parameter K to this uncertainty. Later in this thesis we will discuss something called the post-Newtonian formalism. We will not dive in on this topic here, but at this point the main idea is that the we expand the tt element g_{tt} in the metric in powers of r^{-1}. That way our new g_{tt} will become,

$$-g_{tt} = 1 - \frac{2GM}{rc^2} + 2(GM)^2 \left(\frac{\beta - \gamma}{r^2 c^3} \right) - \frac{K}{c^4} \frac{2(GM)^3}{r^3 c^2} + \mathcal{O}\left(r^{-4}\right) \tag{7}$$

Astrophysical observations in our solar system have already placed strong constraints on β and γ [24]. We can make here the very conservative assumption that the solar-system limits are applicable to the external spacetimes of astrophysical black holes so we can set

$\beta - \gamma = 0$. If the tt element of the black-hole metric has indeed vanishing third term and terminates at the fourth term, the g_{tt} would be [24]

$$-g_{tt} = 1 - \frac{2GM}{rc^2} - \frac{K}{c^4}\frac{2(GM)^3}{r^3c^2} \tag{8}$$

Put this in Eq. (6) and (5) and the size of the black-hole shadow would be

$$r_{sh} = 3\sqrt{3}\frac{GM}{c^2}\left(1 + \frac{1}{9}K\right) \tag{9}$$

From Psaltis et al. [24] we can assume that if there are violations of general relativity there would be this extra $\frac{1}{9}K$ term in the shadow radius and the value of K will be determined by the uncerainty of the radius taken from the picture by EHT. Alternatively to this violation of GR, K could arise from the possible existence of exotic objects like boson stars [19]. We will elaborate on this topic later in the thesis but roughly it means that if GR is correct the central object isn't a black hole but a different object with an non-trivial shape. As will be discussed in section 6.3 of this thesis the value of K measured by EHT will lie between -1.2 and 1.966667

The aim of this thesis is to set bounds on this quantity K by using a very different method, namely by using gravitational waves (GW's) coming from binary black holes. In the next chapters we are going dive into this topic and eventually we are going to compare the bounds on K we get by using GW's with the bounds coming from the EHT picture of a black hole. So, we can determine whether this method for testing GR is more accurate, less accurate or has the same accuracy.

3 Gravitational waves

In this section we are going to elaborate on what gravitational waves (GW's) are and how they come up from the theory of general relativity. This will be done very briefly so readers with no experience in GW physics should consider looking at the references, but the main concepts useful for the rest of the paper will be presented in this section. Also we are going to look at how these GW's are detected.

3.1 Linearized gravity

First to explore gravitational waves we need to discuss the concept of linearized gravity. We do this because the Einstein field equations (EFE) are very hard to solve exactly, so we need to make use of the fact that the black hole to be detected is very far away. This way we can study gravitational waves in the weak-field regime. In that case the spacetime metric $g_{\mu\nu}$ can be written as a flat Minkowski metric of special relativity, $n_{\mu\nu}$,plus some correction due to the weak gravitational fields, $h_{\mu\nu}$:

$$g_{\mu\nu} = n_{\mu\nu} + h_{\mu\nu} \tag{10}$$

where $|h_{\mu\nu}| \ll 1$ is a small metric perturbation [21]

What now follows is a process which involves gauge invariance in which there is a close analogy with the theory of electrodynamics. We will not dive into that process here, but the linearized EFE are gauge-invariant and we can use this gauge freedom to simplify the form of the field equations. For the linearized field equations [21] in the Lorentz gauge we get:

$$\Box\overline{h}_{\mu\nu} = -\frac{16\pi G}{c^4}T_{\mu\nu} \tag{11}$$

Where $\Box$ is the d'Alembertian operator, $\overline{h}_{\mu\nu} = h_{\mu\nu} - \frac{1}{2}\eta_{\mu\nu}h$ and $T_{\mu\nu}$ is the stress-energy tensor.

Writing out the d'Alembertian operator acting on $\overline{h}_{\mu\nu}$ and set $T_{\mu\nu} = 0$ (so source is present) we can see another connection to electromagnetism:

$$\Box\overline{h}_{\mu\nu} = 0 \tag{12}$$

$$\left(-\frac{\partial}{c^2\partial t^2} + \frac{\partial^2}{\partial x^2} + \frac{\partial^2}{\partial y^2}\frac{\partial^2}{\partial z^2}\right)\overline{h}_{\mu\nu} = 0 \tag{13}$$

Which is just the wave equation for waves traveling at the speed of light.
In Eq. (11), $\overline{h}_{\mu\nu}$ is a 4×4 symmetrical matrix and has 10 degrees of freedom. Most of them are not physical and can be eliminated. To do this we use another gauge condition: the transverse-traceless (TT) gauge. The TT gauge is convenient, because it fixes all the local gauge freedom. So the metric perturbation we are left with contains only physical, non-gauge information about the GW radiation. When a plane wave is propagating in the z-direction, the metric perturbation can be written as:

$$h_{ij}^{TT} = \begin{pmatrix} h_+ & h_\times & 0 \\ h_\times & -h_+ & 0 \\ 0 & 0 & 0 \end{pmatrix} \cos[\omega(t - z/c)] \tag{14}$$

This is the transverse-traceless gauge and depends only on two parameters namely: h_+ and $h_\times$ which represent the plus and cross polarization.

3.2 The quadrupole formula

We now want to obtain general solution for the linearized field equation. To do this we use the appropriate Green's function. Then the general solution for $\overline{h}_{\mu\nu}$ is:

$$h_{\mu\nu}^{TT}(t, \mathbf{x}) = \frac{4G}{c^4} \Lambda_{ij,kl}(\hat{\mathbf{n}}) \int_{\mathcal{V}} d^3\mathbf{x'} \frac{T^{kl}(t - |\mathbf{x} - \mathbf{x'}|/c, \mathbf{x'})}{|\mathbf{x} - \mathbf{x'}|} \tag{15}$$

where $\Lambda_{ij,kl}$ is a projection operator which acts like: $h_{\mu\nu}^{TT} = \Lambda_{ij,kl}(\hat{\mathbf{n}}) h^{kl}$.

The integral is taken over a volume $\mathcal{V}$ containing the source, $\hat{\mathbf{n}}$ is the unit vector perpendicular to the wavefront and $|\mathbf{x} - \mathbf{x'}|$ is the distance from the source to the observer. Typically the observer (i.e. the gravitational wave detector) will be very far away from the source. So we can make the approximation: $|\mathbf{x} - \mathbf{x'}| = r$ is the distance to the source. Also we now can introduce the mass quadrupole moment defined as:

$$M^{ij} = \frac{1}{c^2} \int d^3\mathbf{x} T^{00} x^i x^j \tag{16}$$

With this and the approximations made, the gravitational wave seen by the observer is given by:

$$h_{ij}^{TT}(t, \mathbf{x}) = \frac{1}{r} \frac{2G}{c^4} \Lambda_{ij,kl}(\hat{\mathbf{n}}) \ddot{M}^{kl}(t - r/c) \tag{17}$$

This is called the quadrupole formula. Now from Eq. (16) and Eq. (17) we can express the two polarization states h_+ and $h_\times$ as in terms of the mass quadrupole moment:

$$h_+ = \frac{1}{r} \frac{G}{c^4} \left(\ddot{M}_{11} - \ddot{M}_{22} \right) \tag{18}$$

$$h_\times = \frac{2}{r} \frac{G}{c^4} \ddot{M}_{12} \tag{19}$$

3.3 The Newtonian limit

As we can see in Eq. (13), perturbations of the gravitational field propagate at a finite speed c according to the wave equation. This is different in the theory of Newton, in which instantaneous action on a distance can occur. But Newtonian gravity was perfectly capable of describing the world for hundreds of years. So there is a regime in which Newtonian gravity holds and that is when gravitational fields are weak and speeds are small compared to the speed of light ,thus $v \ll c$.

Recall the linearized Einstein equation, Eq. (11). When we look at the stress-energy tensor $T_{\mu\nu}$ we can see that the T_{00} component which is the energy density, is large compared to the momentum-density and the spatial components:

$$T_{00} \sim \rho c^2 \gg T_{i0} \sim \rho v_i c \gg T_{ij} \sim \rho v_i v_j \tag{20}$$

So we can focus on the time-time component $\overline{h}_{00}$ which from the linearized Einstein equations gives:

$$\nabla^2 \overline{h}_{00} \simeq -\frac{16\pi G}{c^4}\rho c^2 \tag{21}$$

Comparing this with the Poisson equation: $\nabla^2\phi = 4\pi G\rho$, we can identify:

$$\overline{h}_{00} \simeq -4\frac{\phi}{c^2} \tag{22}$$

Recall from section 3.1 that $\bar{h}_{\mu\nu} = h_{\mu\nu} - \frac{1}{2}\eta_{\mu\nu}h$, from wich $h_{\mu\nu} = \bar{h}_{\mu\nu} - \frac{1}{2}\eta_{\mu\nu}\bar{h}$. Only $\bar{h}_{00}$ is non-negligible, thus we can write $\bar{h} = \eta^{\mu\nu}\bar{h}_{\mu\nu} \simeq \eta^{00}\bar{h}_{00} = -\bar{h}_{00}$. Now, with $\bar{h}_{00} = -4\frac{\phi}{c^2}$ we can write:

$$\begin{aligned} h_{00} = \bar{h}_{00} - \frac{1}{2}\eta_{00}(-\bar{h}_{00}) = \frac{1}{2}\bar{h}_{00} &= -\frac{2\phi}{c^2} \\ h_{11} = \bar{h}_{11} - \frac{1}{2}\eta_{11}(-\bar{h}_{00}) = 0 + \frac{1}{2}\bar{h}_{00} &= -\frac{2\phi}{c^2} \\ h_{22} &= -\frac{2\phi}{c^2} \\ h_{33} &= -\frac{2\phi}{c^2} \end{aligned} \tag{23}$$

All the off-diagonal elements are zero, e.g. $h_{12} = \bar{h}_{12} - \frac{1}{2}\eta_{12}(-\bar{h}_{00}) = 0$.

Looking at Eq. (10) but only the time-time component we get:

$$g_{tt} = g_{00} = -\left(1 + \frac{2\phi}{c^2}\right) \tag{24}$$

In our situation the potential which has a $1/r^3$ term is given by:

$$\phi = -G\frac{M}{R} + \frac{K}{c^4}\frac{(GM)^3}{R^3} \tag{25}$$

Filling this in the the g_{tt} metric:

$$g_{tt} = -\left(1 - \frac{2GM}{Rc^2} + \frac{K}{c^4}\frac{2(GM)^3}{c^2R^3}\right) \tag{26}$$

3.4 Gravitational wave detection

The first indirect detection of gravitational waves goes back 1974, where Russell Hulse and Joseph Taylor discovered a binary neutron star pair whose orbital period was decreasing over time [20]. This was a first indication that gravitational waves could really exist. In 1971 Rainer Weiss made the first study in what it would take to measure gravitational waves directly by using a interferometer. The basic idea behind this setup is having two long tubes perpendicular to each other and a laser beam running down the tubes. This laser beam is created in a source and then passes to a splitter, creating two beams for the tubes who are precisely out of phase by half a wavelength creating a destructive interference. This way there is no signal at the photodiode where the two beams meet.

As we have seen in Eq. (14) of this chapter, gravitational waves stretch and squeeze space-time in a periodical manner. Now if a gravitational wave passes by then periodically one arm gets stretched and the other compressed, causing a difference in length between the arms. This results in a decrease or increase of the travel length of the beam in the arms causing a misalignment of the beams resulting in a signal of light at the photodiode which can be measured.

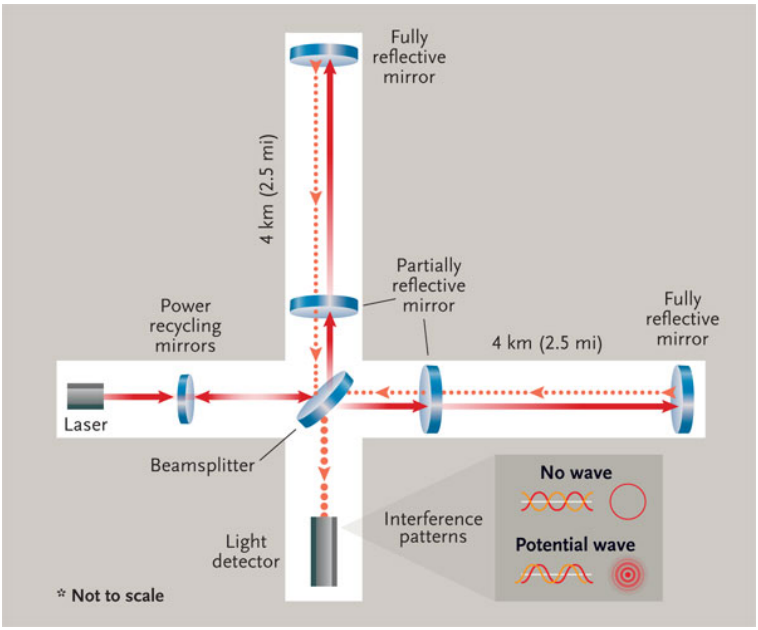

Figure 3: Schematic overview of the GW detector Ligo. Taken from ST: Leah Tiscione [29]

The amount of stretch in the arms is incredibly tiny and is of the order $h \simeq 10^{-21}$ [26]. This means that measurable relative changes in the interferometer arm's length should be smaller: $\frac{\Delta L}{L} \leq 10^{-22}$. This implies that for an interferometer like LIGO with arms of 4 km the difference in length to be measured is $\Delta L = 4km \times 10^{-21} = 4 \times 10^{-18} m$, . Light takes only about 10^{-5}s to go up and down one arm, much less than the typical period of gravitational waves of interest. Therefore, it is beneficial to let the light in the tubes for say 100 trips. This increases its effective path length by 100 and hence the shift in the position of a given phase of the light beam will be of order 10^{-16}m [26].

Because of this incredibly tiny difference in length that has to be measured, the detectors are extremely vulnerable for noise coming from either seismic noise (in the low frequency range), or thermal vibrations in the suspended wires (at mid-range frequency) and at the high frequency, quantum mechanics plays a role in fluctuating amount of photons hitting the mirrors at the end of the tubes causing noise at the high frequency range.

So, a lot of fine tuning went into the project after the start of the first interferometer in 2002 [5]. The one thing that is especially beneficial to the accuracy is using multiply detectors. As LIGO consist of two detectors, one located in Livingstone(Louisiana) and one in Hanford(Washington), it is able to distinguish noise from a gravitational wave by comparing the two outcomes of both detectors. To put in simply: If one gives a signal and the other don't it is impossible that is was a gravitational wave, because it would strike the two detectors almost simultaneously. This way the first measurement of a gravitational wave was made by the Advanced LIGO detectors [8], this event was: GW150914, a binary black hole merger.

Besides LIGO the only interferometer which has detected gravitational waves is Virgo located in Santo Stefano a Macerata (Italy). In 2017 it was announced that a first gravitational wave GW170814 by both LIGO and Virgo was detected [7].

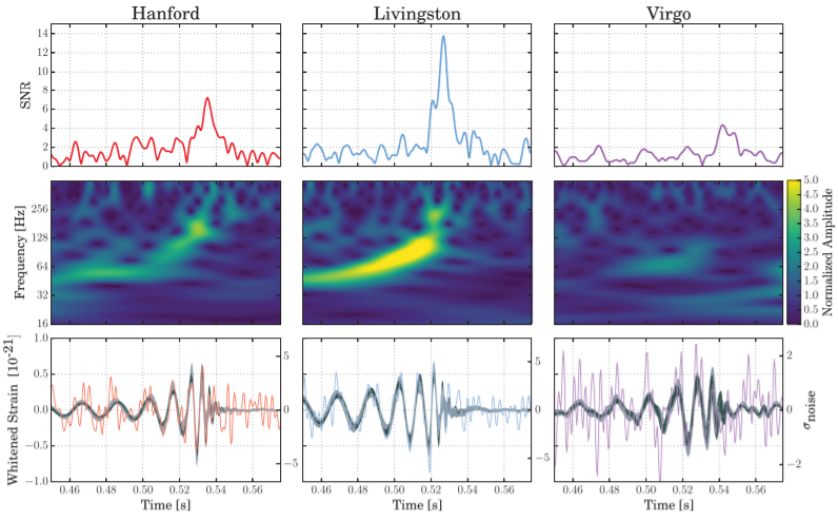

Figure 4: The GW event GW170814 observed by LIGO Hanford, LIGO Livingston, and Virgo. [**?**]

GEO600 in Germany and KAGRA in Japan are both operational at this time but have not been detecting any gravitational waves up to this point, but KAGRA is designed to have a sensitivity equal or greater than LIGO, so detections are expected for KAGRA in the future.

For the future there are plans for making a very large interferometer called the Einstein telescope which would have arms of 10km. Also this detector will be built underground, drastically reducing the seismic noise so it will be capable of detecting gravitational waves with bigger wavelengths [25]. There is also a plan for an even larger interferometer in space called LISA which consists of 3 satellites orbiting around the sun with a distance of 2.5 million kilometres between each satellite. In the low-frequency gravitational wave domain,

below one Hertz, we expect to observe the heaviest and most distant objects and this will be obtainable by LISA. [11]. .

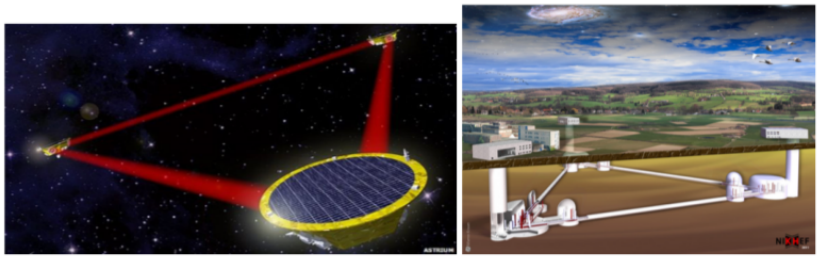

Figure 5: Detectors that are planned for the future. Left: The space-based Laser Interferometer Space Antenna LISA. Right: The underground observatory Einstein Telescope, which may be built in the Dutch-Belgian-German border region.

4 Gravitational waves from binary systems

Until now the only detections made are from compact binary systems such as binary black holes or binary neutron stars. In these systems two black holes of two neutron stars are revolving around each other creating gravitational waves. This revolving of to massive objects is called inspiral. In this process the two objects orbit some common centre of gravity in which they emit gravitational waves which carry some amount of energy [21]. Because this energy is taken away from the system the orbits will shrink. As two black holes are close to each other the frequency of the gravitational waves emitted are high enough that they can be detected by our interferometers. This means that GWs that currently can be detected are from the late stages of inspiral, which are called the merger and the ringdown. In this merger phase of the binary's existence, the orbits become increasingly smaller over time so the frequency and amplitude of the GWs are high enough to be detected by the interferometers. Eventually this merger phase results in an final state called ringdown, in which the two black holes become one. In this stage, the newly formed single black hole or neutron star undergoes some damped oscillations as a result from the merger phase.

4.1 Signal from an inspiraling binary

To put a mathematical frame work for the binary system, we have to make use of the fact that gravitational waves carry away angular momentum from the system. This causes the orbits to become more and more circular. So our situation becomes a classic two-body problem in which to objects orbit around each other with a fixed radius R. Also, we can assume that the orbital frequency ω and the distance R between the two objects does not change much over a single orbit (adiabatic approximation). This leaves us with a classic two-body problem.

Consider two masses m_1 and m_2 which we treat as point-like particles with positions $\mathbf{x}_1(t)$ and $\mathbf{x}_2(t)$. Then we get [22]:

$$\mathbf{x}_1(t) = \frac{m_2}{m_1 + m_2} R\hat{\mathbf{e}}(t) = \frac{\mu}{m_1} R\hat{\mathbf{e}}(t) \tag{27}$$

$$\mathbf{x}_2(t) = -\frac{m_1}{m_1 + m_2} R\hat{\mathbf{e}}(t) = -\frac{\mu}{m_2} R\hat{\mathbf{e}}(t) \tag{28}$$

where $\mu = \frac{m_1 m_2}{m_1+m_2}$ and $\hat{\mathbf{e}}(t)$ is the orientation vector given by:

$$\hat{\mathbf{e}}(t) = (\cos(\omega t), \cos(\iota)\sin(\omega t), \sin(\iota)\sin(\omega t)) \tag{29}$$

where ι is the angle of inclination of the angular velocity of the system with respect to the z-axis which is chosen to point at the observer. $\hat{\mathbf{e}}$ is a unit vector pointing from the centre of mass m_2 to the object with mass m_1.

Now, for determining a GW signal we have to use the formula for the quadrupole moment Eq. (16) defined in section 3.2. If we use $T^{00} = \rho c^2$ we can rewrite Eq. (16) as:

$$M^{ij}(t) = \frac{1}{c^2} \int d^3\mathbf{x} \rho(t, \mathbf{x}) x^i x^j, \tag{30}$$

where the mass density $\rho(t, \mathbf{x})$ is defined as:

$$\begin{aligned} \rho(t, \mathbf{x}) &= m_1 \delta^3(\mathbf{x} - \mathbf{x}_1(t)) + m_2 \delta^3(\mathbf{x} - \mathbf{x}_2(t)) \\ &= m_1 \delta^3 \left(\mathbf{x} - \frac{\mu}{m_1} R\hat{\mathbf{e}}(t) \right) + m_2 \delta^3 \left(\mathbf{x} + \frac{\mu}{m_2} R\hat{\mathbf{e}}(t) \right) \end{aligned} \tag{31}$$

after performing the integration with (28), we get

$$M^{ij}(t) = \left[m_1 \frac{\mu^2}{m_1^2} R^2 + m_2 \frac{\mu^2}{m_2^2} R^2 \right] \hat{e}^i \hat{e}^j = \mu R^2 \hat{e}^i \hat{e}^j \tag{32}$$

Now if we put this in the two polarization states, formula (18) and (19). We get after some more algebra the following expressions:

$$h_+ = -\frac{4}{r} \frac{G\mu R^2 \omega^2}{c^4} \frac{1 + \cos^2(\iota)}{2} \cos(2\omega t_{ret}) \tag{33}$$

and

$$h_\times = -\frac{4}{r} \frac{G\mu R^2 \omega^2}{c^4} \cos(\iota) \sin(2\omega t_{ret}) \tag{34}$$

Where $t_{ret} = t - r/c$ is the retarded time. That is the time corrected for our detectors on a distance r from the binary system. It comes from Eq. (17) where $\ddot{M}^{kl}$ depends on this quantity.

Now from Kepler's third law we can see that R, ω and M are not independent quantities [22].

$$R^2 = \frac{GM}{\omega^2} \tag{35}$$

where $M = m_1 + m_2$, and we assumed that the two particles are far apart from each other.

Together with the chirp mass defined as

$$\mathcal{M}_{chirp} = \frac{(m_1 m_2)^{3/5}}{(m_1 + m_2)^{1/5}} \tag{36}$$

we can write the equations for the two polarizations in a more convenient form.

$$h_+ = -\frac{4}{r}\left(\frac{G\mathcal{M}_{chirp}}{c^2}\right)^{5/3}\left(\frac{\omega}{c}\right)^{2/3}\frac{1+\cos^2(\iota)}{2}\cos(2\omega t_{ret}) \tag{37}$$

$$h_\times = -\frac{4}{r}\left(\frac{G\mathcal{M}_{chirp}}{c^2}\right)^{5/3}\left(\frac{\omega}{c}\right)^{2/3}\cos(\iota)\sin(2\omega t_{ret}) \tag{38}$$

If we now want to translate this to a certain measure for the strain in the detectors arms we have to take into account the orientation of the binary in space in terms of spherical coordinates.

After some calculation with the rotation matrix we can write the strain h as in terms of the + and × polarizations [21]

$$h = F_+(\theta,\phi,\psi)h_+ + F_\times(\theta,\phi,\psi)h_\times \tag{39}$$

where θ,ϕ and ψ represent the spherical coordinates that give the orientation of the binary in space. F_+ and $F_\times$ are called the beam pattern functions and are defined as:

$$F_+(\theta,\phi,\psi) = \frac{1}{2}(1+\cos^2\theta)\cos 2\phi\cos 2\psi - \cos\theta\sin 2\phi\sin 2\psi \tag{40}$$

and

$$F_\times(\theta,\phi,\psi) = \frac{1}{2}(1+\cos^2\theta)\cos 2\phi\cos 2\psi + \cos\theta\sin 2\phi\sin 2\psi \tag{41}$$

Now after collecting the common prefactors in Eq. (37) and Eq. (38) and represent them by $A(t)$ we get:

$$h(t) = A(t)\sqrt{F_+^2(1+\cos^2(\iota))^2 + F_\times^2 4\cos^2(\iota)}\cos(\Phi(t)+\varphi_0) \tag{42}$$

where we have written $2\omega t_{ret}$ as $\Phi(t)$ and φ_0 is defined as:

$$\varphi_0 = \arctan\left(\frac{-F_\times 2\cos(\iota)}{F_+(1+\cos^2(\iota))}\right) \tag{43}$$

4.2 The stationary phase approximation

For the data analysis of GW's we use something called matched filtering, this enables us to get a signal out of a lot of noise. But matched filtering requires the Fourier transform of the strain, so that is in the frequency-domain instead of the time-domain. To do this we have to use an approximation: the stationary phase approximation.

First we take the Fourier transform of $h(t)$ and for convenience we will not include the orientation of the binary (the square root term in Eq. (42)), as it is not affected by the Fourier transform

$$\begin{aligned}\tilde{h} = \int_{-\infty}^{\infty} h(t)e^{2\pi i f t}dt &= \frac{1}{2}\int_{-\infty}^{\infty} dtA(t)\left(e^{i(\Phi(t)+\varphi_0)} + e^{-i(\Phi(t)+\varphi_0)}\right)e^{2\pi i f t} \\ &= \frac{1}{2}\int_{-\infty}^{\infty} dtA(t)\left(e^{i(2\pi f t+\Phi(t)+\varphi_0)} + e^{i(2\pi f t-\Phi(t)-\varphi_0)}\right)\end{aligned} \tag{44}$$

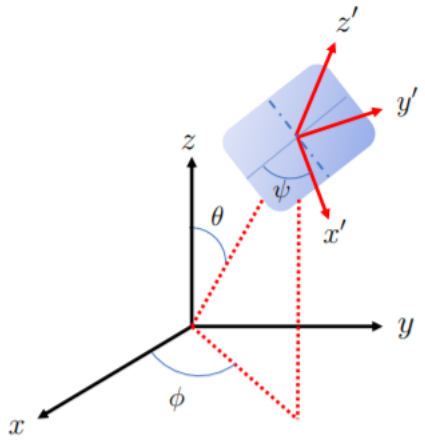

Figure 6: A schematic overview of the spherical orientation of a GW. The wave propagates is the z' direction which is at angles (θ, ϕ) with respect to the unprimed coordinates.

where we made use of the Euler formula to write the cosine term in terms of e. Considering the term $e^{i(2\pi ft+\Phi(t)+\varphi_0)}$ as the unit vector in the complex plane, $2\pi ft + \Phi(t) + \varphi_0$ is than the angle with respect to real axis. Because it will only increase over time, since t is only increasing, this term will average out over zero, so we can neglect it.

$$\tilde{h} \simeq \frac{1}{2} e^{-i\varphi_0} \int_{-\infty}^{\infty} dt A(t) e^{i(2\pi ft - \Phi(t))} \tag{45}$$

Now the idea behind stationary phase approximation is that we only evaluate the integral near the stationary point $t = t_s$. We can do this because this t_s has the largest contribution to the integral.
We can Taylor expand the exponent in Eq. (45) around $t = t_s$ up to quadratic order to get:

$$2\pi ft - \Phi(t) = 2\pi ft_s - \Phi(t_s) + 2\pi f(t - t_s) - \dot{\Phi}(t_s)(t - t_s) - \frac{1}{2}\ddot{\Phi}(t_s)(t - t_s)^2 \tag{46}$$

where, $2\pi f(t - t_s) - \dot{\Phi}(t_s)(t - t_s) = 0$ because $2\pi f = \dot{\Phi}(t_s)$
If we then also define, $x = \sqrt{\frac{\ddot{\Phi}}{2}}(t - t_s)$ we get

$$\tilde{h}(f) \sim \frac{1}{2} A(t_s) e^{-i\varphi_0} e^{-i(2\pi ft_s - \Phi(t_s))} \left(\frac{2}{\ddot{\Phi}(t_s(f))} \right) \int_{-\infty}^{\infty} dx e^{-ix^2} \tag{47}$$

Here $\int_{-\infty}^{\infty} dx e^{-ix^2}$ is a Guassian integral with a standard solution:

$$\int_{-\infty}^{\infty} dx e^{-ix^2} = \sqrt{\pi} e^{-i\pi/4} \tag{48}$$

this gives us the final result,

$$\tilde{h}(f) = \frac{\sqrt{\pi}}{2} A(t(f)) e^{-i\varphi_0} \left(\frac{2}{\ddot{\Phi}(t(f))} \right) e^{i\Psi(f)} \tag{49}$$

with $\Psi(f) = 2\pi f t(f) - \Phi(t(f)) - \frac{\pi}{4}$, where we note that for a given frequency f, one has $t_s = t(f)$

4.3 The post-Newtonian formalism

In later stages of the inspiral (but still weak field regime) the approximations made till this point are not sufficient. We come closer to the relativistic regime and therefore we have to expand Eq. (49) with some power series of an additional parameter which is given by the velocity divided by the speed of light, v/c. For this to be feasible we still need the binary inspiral to be adiabatic so the change in orbit is very small compared to the time scale of the inspiral.
Above we only considered gravitational waves at leading order of v/c. But every higher order term in this post-Newtonian expansion is a perturbation arising from the general relativistic effects. That way we get a greater accuracy without having to solve the EFE exactly. At the point of merger and plunge of the inspiral we need to numerically treat the full EFE, but until this point the post-Newtonian formalism is widely used to accurately describe the GWs created by inspiralling compact binaries.

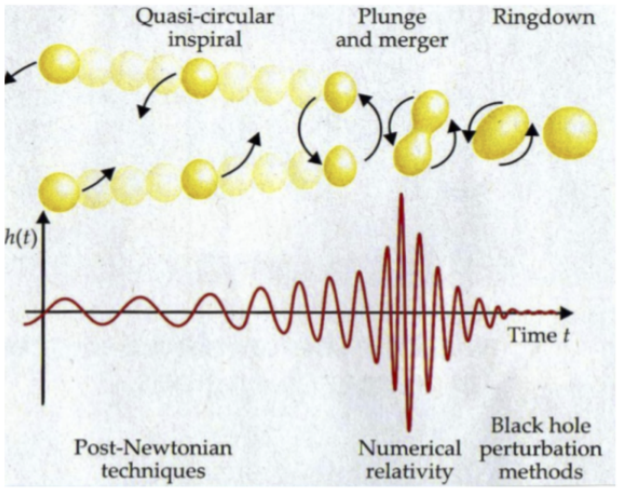

Figure 7: The inspiral-merger-ringdown process for two black holes (top), and the shape of the gravitational wave that is produced (bottom, in red) [13]. Post-Newtonian formalism holds until the last stable circular orbit.

Now, for higher order the Fourier transformed frequency domain waveform is given by [15, 16]

$$\tilde{h} = \mathcal{A} f^{-7/6} e^{i\Psi(f)} \tag{50}$$

where $\mathcal{A} \propto \mathcal{M}^{5/6} Q(angles)/r$. Here $Q(angles) = Q(\iota, \theta, \phi, \psi)$ is the square root from Eq. (42) and $\Psi(f)$ is the phase which is up to the 3.5 PN given by,

$$\Psi(f) = 2\pi f t_c - \phi_c - \frac{\pi}{4} + \frac{3}{128\eta(v/c)^5} \sum_{k=0}^{7} \phi_k (v/c)^k \tag{51}$$

where the dimensionless quantity $\eta = m_1 m_2/(m_1 + m_2)^2$ is the symmetric mass ratio, t_c is the time of coalescence, which is the time at which the frequency formally diverges: $t \to tc$ implies $f_{gw} \to \infty$. From Kepler's third law, this implies that the separation between the point particles goes to zero: $R \to 0$. and ϕ_c is the phase of coalescence
In principle there infinitely many terms instead of 7 but these are the terms that are calculated until current times. For a list of all the coefficients see [12]. For historical reasons we call the seventh coefficient the 3.5 PN order, so generally: $(v/c)^n$ corresponds to $n/2PN$ order.

5 Binary inspiral in a modified gravitational potential

In this thesis we will explore the 2PN contribution from the post-Newtonian formalism to test general relativity. In this chapter will set the mathematical framework using Lagrangian mechanics to get to an understanding of what a 2PN term means for the energy of a binary system. And how an $1/R^3$ correction in the potential lead to this 2PN term. Also we are going to touch upon the possibility of the existence of boson stars.

5.1 Langrangian for binary motion and the radius

For our Langrangian we have:

$$L = T - V \tag{52}$$

were the potential is coming from the standard law of gravitation of Newton with an extra $1/r^3$ and r is just the radius of some binary system. That gives us for the potential V:

$$V_R = -G\frac{M}{r} - \frac{K}{c^4}\frac{G^3 M^3}{r^3} \tag{53}$$

here K is some dimensionless parameter on which we can place a certain bound on, that is what we will do later in this thesis. c is the speed of light.
T is the kinetic energy of the system which consists of the kinetic energy for both the two separate masses m_1 and m_2.

$$T = \frac{1}{2} m_1 v_1^2 + \frac{1}{2} m_2 v_2^2 \tag{54}$$

Recall Eq. (27) and Eq. (28) and we can write this in terms of the reduced mass, the frequency ω and the radius R:

$$T = \frac{1}{2}m_1\left(\frac{\mu}{m_1}r\omega\right)^2 + \frac{1}{2}m_2\left(\frac{\mu}{m_2}r\omega\right)^2 \tag{55}$$

Now we can put in the definition for the reduces mass $\mu = m_1m_2/(m_1+m_2)$ back in and after rewriting we get

$$T = \frac{1}{2}\frac{m_1m_2}{M}r^2\omega^2 = \frac{1}{2}\mu r^2\omega^2 \tag{56}$$

Now with these expressions for the kinetic and potential energy we can use the Euler-Lagrange equations to eventually get an expression for the radius r in terms of G,M,ω and K.
The Euler-Lagrange equations:

$$\frac{\partial L}{\partial r} - \frac{d}{dt}\frac{\partial L}{\partial \dot{r}} = 0 \tag{57}$$

Putting in the Langrangian $L = T - V$ and assuming this is all in the adiabatic limit so $\dot{r} = 0$ (the change in orbit is small) we get

$$\mu r\omega^2 - \frac{G\mu M}{r^2} - 3\frac{K}{c^4}\mu\frac{G^3M^3}{r^4} = 0 \tag{58}$$

where we can write r as:

$$r(\omega) = r_0(\omega)(1+\delta r(\omega)) \tag{59}$$

where $\delta r(\omega)$ is small: $\delta r(\omega) \ll 1$. Putting this expression for $r(\omega)$ in Eq. (58) we get

$$\mu r_0(1+\delta r)\omega^2 - \frac{1}{r_0^2}G\mu M(1-2\delta r) - 3\frac{1}{r_0^4}\frac{K}{c^4}\mu(GM)^3(1-4\delta r) \tag{60}$$

Here we made use of the fact that δr is small so we could Taylor expand: $\frac{1}{r^2} = \frac{1}{r_0^2}(1-2\delta r)$ and $\frac{1}{r^4} = \frac{1}{r_0^4}(1-4\delta r)$.

From Kepler's law Eq. (35) we get

$$r_0(\omega) = M^{1/3}\omega^{-2/3}G^{1/3} \tag{61}$$

Putting this in Eq. (60) and assume K and δr are small so $K\delta r \simeq 0$, we get

$$\begin{aligned}\mu G^{1/3}M^{1/3}\omega^{-2/3}(1+\delta r)\omega^2 - G\mu M M^{-2/3}G^{-2/3}\omega^{4/3}(1-2\delta r) \\ -3M^{-4/3}\omega^{8/3}G^{-4/3}\frac{K}{c^4}\mu(GM)^3(1-4\delta r) = 0\end{aligned} \tag{62}$$

Rewriting this gives us an expression for δr:

$$\delta r = \frac{K}{c^4}(GM)^{4/3}\omega^{4/3} \tag{63}$$

And with this we can write

$$r(\omega) = (GM)^{1/3}\omega^{-2/3}\left(1 + \frac{K}{c^4}(GM\omega)^{4/3}\right) \tag{64}$$

5.2 Total energy of the system as function of the frequency

For the total energy we have,

$$E = T + V \tag{65}$$

that gives us

$$E = \frac{1}{2}\mu R^2\omega^2 - \frac{G\mu M}{R} - \frac{K}{c^4}\mu\left(\frac{GM}{R}\right)^3 \tag{66}$$

here we can insert Eq. (64) with $R = r(\omega)$ which gives us the following expression

$$E = \frac{1}{2}\mu\omega^2\left[1+\frac{K}{c^4}(GM\omega)^{4/3}\right]^2(GM)^{2/3}\omega^{-4/3} - G\mu M\left[1+\frac{K}{c^4}(GM\omega)^{4/3}\right]^{-1}(GM)^{-1/3}\omega^{2/3} - \frac{K}{c^4}\mu(GM)^3(GM)^{-1}\omega^2\left[1+\frac{K}{c^4}(GM\omega)^{4/3}\right]^{-3} \tag{67}$$

here we can again use Taylor expansions for the terms in between the square brackets.

$$E = \frac{1}{2}\mu\omega^{2/3}(GM)^{2/3}\left[1+\frac{2K}{c^4}(GM\omega)^{4/3}\right] - \mu(GM)^{2/3}\omega^{2/3}\left[1-\frac{K}{c^4}(GM\omega)^{4/3}\right] - \frac{K}{c^4}\mu(GM)^2\omega^2\left[1-\frac{3K}{c^4}(GM\omega)^{4/3}\right] \tag{68}$$

Rewriting this gives us the following expression

$$E(\omega) = -\frac{1}{2}\mu(GM\omega)^{2/3}\left[1-\frac{2K}{c^4}(GM\omega)^{4/3}\right] \tag{69}$$

5.3 The energy-balance equation

From the stationary phase approximation (recall Eq. (49)) we can get that the phase is given by:

$$\Psi(f) = 2\pi f t(f) - \phi(t(f)) - \pi/4 \tag{70}$$

Then we can take the derivative with respect to the frequency:

$$\frac{d\Psi(f)}{df} = 2\pi t(f) + 2\pi f\frac{dt(f)}{df} - \frac{d\phi(t(f))}{df} \tag{71}$$

Making use of the chain rule here and notice that $2\pi f = \dot{\phi}(t(f))$ so the last two terms cancel out and we are left with:

$$\frac{d\Psi(f)}{df} = 2\pi t(f) \tag{72}$$

Taking the derivative again with respect to f and use the chain rule gives us

$$\frac{d^2\Psi(f)}{df^2} = 2\pi\frac{dt(f)}{df} = 2\pi\frac{dt(f)}{dE}\frac{dE}{df} = 2\pi\left(\frac{dE}{df}/\frac{dE}{dt}\right) \tag{73}$$

so,

$$\frac{d^2\Psi}{d\omega^2} = 2\frac{dE/d\omega}{\dot{E}_{gw}} \tag{74}$$

5.4 Finding the 2PN order in the phase

Now we are going to use Eq. (74) to find the phase with our $1/r^3$ term in the potential. To do that we have to define $\dot{E}_{gw}$. Following GR we get for $\dot{E}_{gw}$ [21]:

$$\dot{E}_{gw} = -\frac{32}{5}\frac{G}{c^5}\mu^2(GM)^{4/3}\omega^{10/3} \tag{75}$$

- But this expression could be wrong if GR is violated. In this thesis we are testing GR and thus, it has to pointed out that we get a different expression for this GW energy in that case.
- In chapter 2 we already mentioned the term boson star. This is the alternative to the GR violation which means that this expression for $\dot{E}_{gw}$ is perfectly fine but we are not dealing with binary black holes but with some strange objects called boson stars. These hypothetical objects would consist mainly of boson particles and it's scalar field for the potential would have a non-trivial multipolar structure [19], see figure 8. Hence the deviation from 2PN term.

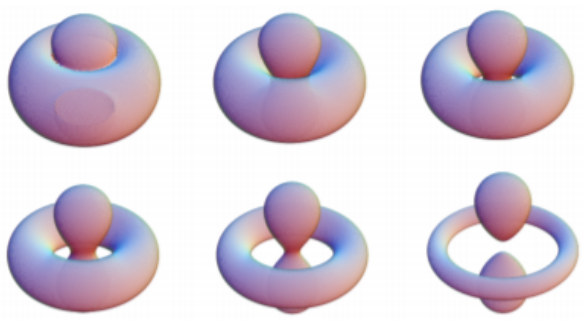

Figure 8: Surfaces of constant energy density for a certain potential of the boson star [19]

We already derived the expression for the total energy as a function of the frequency ω. Rewriting Eq. (69) gives us

$$E(\omega) = -\frac{1}{2}\mu(GM\omega)^{2/3} + \frac{K}{c^4}\mu(GM\omega)^2 \tag{76}$$

Taking the derivative

$$\frac{dE(w)}{d\omega} = -\frac{1}{3}\mu(GM)^{2/3}\omega^{-1/3} + \frac{2K}{c^4}\mu(GM)^2\omega \tag{77}$$

Now we can put this in Eq. (74):

$$\frac{d^2\Psi}{d\omega^2} = 2\frac{dE/d\omega}{\dot{E}_{gw}} = 2\frac{1}{3}\frac{5}{32}\frac{c^5}{G}\mu^{-1}(GM)^{-2/3}\omega^{-11/3}\left[1 - 6\frac{K}{c^4}(GM)^{4/3}\omega^{4/3}\right] \tag{78}$$

Here we can again introduce the chirp mass see Eq. (36) to rewrite this as:

$$\frac{d^2\Psi}{d\omega^2} = \frac{5}{48}G^{-5/3}c^5\mathcal{M}_{chirp}^{-5/3}\omega^{-11/3} - \frac{5}{8}\frac{K}{c^4}G^{-1/3}c^5\mathcal{M}_{chirp}^{-1/3}\omega^{-7/3} \tag{79}$$

Taking the integral twice of this expression gives us

$$\Psi = \frac{3}{128}c^5G^{-5/3}\mathcal{M}_{chirp}^{-5/3}\omega^{-5/3} - \frac{45}{32}\frac{K}{c^4}c^5G^{-1/3}\mathcal{M}_{chirp}^{-1/3}\omega^{-1/3} + C\omega + D \tag{80}$$

where C and D are integration constants which represents the reference time and reference phase respectively and can both be set to zero for that reason.
Now we can use the symmetric mass ratio defined by: $\eta = m_1m_2/M^2$ and that $v/c = (\pi GMf/c^3)^{1/3}$, after rewriting our expression of the phase becomes,

$$\Psi = \frac{3}{128\eta(v/c)^5}\left[1 - 60K\left(\frac{v}{c}\right)^4\right] \tag{81}$$

If we compare this with Eq. (51) we have for ϕ_4 the normal GR part plus a correction of $-60K$. If we set the second PN term $\phi_4 \to (1 + \delta\phi_4)\phi_4$ we get

$$-60K = -\delta\phi_4\phi_4 \tag{82}$$

so

$$K = -\frac{1}{60}\delta\phi_4\phi_4 \tag{83}$$

where [12]

$$\phi_4 = 10\left(\frac{3058673}{1016064} + \frac{5429}{1008}\eta + \frac{617}{144}\eta^2\right) \tag{84}$$

6 Testing GR with gravitational waves

In this section we discuss how the data analysis of gravitational wave events works and how the data that comes out of the GW detectors can be translated into useful information.

6.1 Parameter estimation

The goal of data analysis of gravitational waves is to get some real values for certain parameters that we are interested in from the observed data. To do this use a statistical technique called Bayesian statistics, in which we use prior knowledge about an event and the data that is obtained from experiments.
From previous obtained knowledge of binary black holes we can make some educated guesses to make a certain hypothesis we call $\mathcal{H}$. With that we can define the posterior probability density which is the probability that we get certain parameters given some data and hypothesis

$$p(\bar{\theta}|d,\mathcal{H}) \tag{85}$$

where for a compact binary black hole $\bar{\theta} = (m_1, m_2, \mathbf{S}_1, \mathbf{S}_2, \alpha, \delta, \iota, \psi, d_L, t_c, \phi_c)$ are the parameters which consists of the masses m_1 and m_2 and the spins $\mathbf{S}_1$ and $\mathbf{S}_2$ of the binary and the angles $\alpha, \delta, \iota, \psi$ that make up the orientation with respect to a detector. d_L is the luminosity distance and t_c and ϕ_c are the time and phase of coalescence respectively. $\mathcal{H}$ is the hypothesis and d are the detector date. Extra parameters can be added, e.g. the deviation of the 2PN term $\delta\phi_4$ which is what we will do in this thesis.

Now we are going to use Bayes' theorem:

$$p(A|B) = \frac{p(B|A)p(A)}{p(B)} \tag{86}$$

Which gives the probability of A given B. Using this theorem we can write the posterior probability density function:

$$p(\bar{\theta}|\mathcal{H},d) = \frac{p(d|\mathcal{H},\bar{\theta})p(\bar{\theta}|\mathcal{H})}{p(d|\mathcal{H})} \tag{87}$$

where $p(d|\mathcal{H},\bar{\theta})$ is called the likelihood which we will discuss later, $p(\bar{\theta}|\mathcal{H})$ is the prior probability density which is a function we will choose based on what we know before any measurement takes place and $p(d|\mathcal{H})$ is the evidence for the hypothesis e.g. the sum of all possibilities for set of data given the hypothesis. As can be seen $p(d|\mathcal{H})$ doesn't depend on the parameters and is set by the requirement that the posterior probability density is to be normalized.

For calculating the likelihood we can split the data up in some noise contribution and some signal contribution so we can write it as: $d(t) = n(t) + h(\bar{\theta}, t)$ with $h(\bar{\theta}, t)$ is assumed to be known following from the definition of $p(d|\mathcal{H},\bar{\theta})$. Furthermore, we assume that the noise $n(t) = d(t) - h(\bar{,}t)$ is stationary and follows a Gaussian distribution, so we can write the probability distribution for the noise as [2]

$$p[n] = \mathcal{N}e^{-\frac{1}{2}(n|n)} \tag{88}$$

Here $\mathcal{N}$ is a normalization factor and we used the noise-weighted inner product defined as:

$$(A|B) = 4\mathcal{R}\int_0^\infty df \frac{\tilde{A}^*(f)\tilde{B}(f)}{S_n(f)} \tag{89}$$

Where $\tilde{A}^*$ and $\tilde{B}$ are the complex conjugate of the Fourier transformed functions and $S_n(f)$ is the noise spectral density. It assigns the power of the noise as a function of the frequency. In our case $\tilde{n}(f) = \tilde{d}(f) - \tilde{h}(\bar{\theta}, f)$. Putting this is Eq. (88) will give us the likelihood

$$p(d|\mathcal{H}, \bar{\theta}) = \mathcal{N} e^{-\frac{1}{2}(d-h(\bar{\theta})|d-h(\bar{\theta}))} \tag{90}$$

Now with this likelihood function and the other terms in Eq. (87) assumed to be known we can in principle calculate the posterior probability density function. However, our parameter space consists of 15 parameters (including all vector directions for the spin) and due to this high number of dimensions it will be very hard to compute. We want to somehow bring the number of parameters back to one with a technique called nested sampling [27].

6.2 Nested Sampling

If we take the integral on both sides at Eq. (87) then we get

$$\int d^N\bar{\theta} p(\bar{\theta}|d, \mathcal{H}) p(d|\mathcal{H}) = p(d|H) = \int d^N\theta p(d|\mathcal{H}, \bar{\theta}) p(\bar{\theta}|\mathcal{H}) \tag{91}$$

Here we used that the evidence does not depend on $\bar{\theta}$ and $p(\bar{\theta}|\mathcal{H}, d)$ is normalized by definition. The idea behind nested sampling is that we rewrite the above integral in terms of a single scalar called the prior mass. First we write:

$$p(d|H) = \int d^N\theta p(d|\mathcal{H}, \bar{\theta}) p(\bar{\theta}|\mathcal{H}) = \int d^N\theta L(\bar{\theta}) \pi(\bar{\theta}) \tag{92}$$

Where $L(\bar{\theta})$ replaced the likelihood function and $\pi(\bar{\theta})$ the prior probability distribution. Now we define the prior mass X as a scalar that represents the fraction of the prior volume with a likelihood greater than some value λ.

$$x(\lambda) = \int_{L(\bar{\theta})>\lambda} dX \tag{93}$$

Where $\pi(\bar{\theta}) d^N\theta = dX$. So, the prior mass is the prior integrated over a hypervolume in N-dimensional parameter space, which is bounded by a hypersurface of lowest likelihood $L(\bar{\theta}) = \lambda$. since the prior mass is normalized we have $X \in [0, 1]$, so for $X = 0$ we have the surface within which there are no points with a highter likelihood: $\lambda = L_{max}$, and for $X = 1$ we have the surface within which all points have higher likelihood: $\lambda = L_{min}$
Using this prior mass we can rewrite the evidence integral from Eq. (92) as Z:

$$Z = \int \int ... \int L(\bar{\theta}) \pi(\bar{\theta}) d\bar{\theta}^N \tag{94}$$

What we now want is to construct a function $\tilde{L}(X)$ by finding locations $\bar{\theta}_k$ in parameter space with progressively higher likelihood L_k and hence progressive smaller prior mass X_k. We can approximate the evidence integral Z by swithing to a summation,

$$Z \simeq \sum_{k=1} L_k \Delta X_k \tag{95}$$

Looking back at Eq. (87) we can see then see that we can write the posterior probability density as

$$p(\bar{\theta}|\mathcal{H}, d) \simeq \frac{L_k}{Z}\Delta X_k \tag{96}$$

Now the algorithm of nested sampling works as follows:

1. First drop say M random samples across parameter space drawn from the prior $\pi(\bar{\theta})$ we call these live points with each a value for the likelihood $L(\bar{\theta}_1), ..., L(\bar{\theta}_M)$.

2. Discard the live point with the lowest likelihood i.e. the highest prior mass.

3. Replace with a new live point which has a higher likelihood than the lowest remaining one.

4. Some different point within the new set of live points is now associated with the lowest likelihood and we can repeat the step above.

5. When the termination condition is reached, calculate the evidence.

After we discard the lowest-likelihood point, we have to assign a new prior mass to the new lowest-likelihood live point. We can do this statistically and by making an educated guess drawn from a distribution.
This is how that is done: say we have just discarded the lowest likelihood point, then the new lowest likelihood point has to be assigned to a prior mass. The probability that the surface with highest prior mass is at $X = \chi$ is the joint probability that none of the samples have a prior mass $X > \chi$. Since the live points are uniformly sampled from the prior mass and therefore the prior mass is uniform in $[0, 1]$, we can write the probability as

$$P(X_i < \chi) = \prod_{i=1}^{M} \int_0^{\chi} dX_i = \prod_{i=1}^{M} \chi = \chi^M \tag{97}$$

The probability density that the highest of M samples has prior mass χ is then

$$P(\chi_i, M) = M\chi^{M-1} \tag{98}$$

which is just the derivative of Eq. (97). For determining how long the algorithm runs until termination we can define something called the shrinkage ratio between the new and the old highest prior mass as: $t = X_1/X_0$. This has the same probability density:

$$p(t, M) = Mt^{m-1} \tag{99}$$

We can now draw a shrinkage ratio from Eq. (99) and multiply it by the old prior mass, i.e. $X_k = t_k X_{k-1}$. Starting of with $X_0 = 1$, at the k_{th} iteration the live point with the largest prior mass is given by:

$$X_k = \prod_{j=1}^{k} t_j \tag{100}$$

Recall Eq. (99) the mean and standard deviation of $\ln(t)$ then go as:

$$\ln(t) \sim (-1 \pm 1)/M \tag{101}$$

and the mean and standard deviation of $\ln(X_k)$ go as

$$\ln(X_k) \sim (-k \pm \sqrt{k})/M \tag{102}$$

Hence the mean values of X_k will go like:

$$\langle X_k \rangle = \exp(-k/M) \tag{103}$$

From this last equation we see that the prior mass where the likelihood is the largest is reached exponentially quick and the errors decrease exponentially.

When does the algorithm end? For the the termination condition there is no natural choice, but in practice we can estimate the amount of evidence still to be accumulated as current largest likelihood among live points, $L_{max,cur}$ times the current largest prior mass $X_{max,cur}$. Then we compare this with the some small value which in our case is 0.001,

$$L_{max,cur} X_{cur} < 0.001 \tag{104}$$

The reason why the right hand side is set to this value is that it is much smaller than the typical evidences obtained for a detectable gravitational wave, which ranges between $10s$ and $100s$ [31].

6.3 Parameterized tests of general relativity

Now with the method described in the last two sections we can get a posterior probability density function by adding a parameter to $\bar{\theta}$ which represents the deviation from ϕ_4 called $\delta\phi_4$. Then with the help of nested sampling we get a distribution for $\delta\phi_4$ and thus for K, see Eq. (83).

We use a python code to evaluate the data coming from detections of both Advanced LIGO and Advanced Virgo which are publicly available [1], as collected in the catalog GWTC-1 [6]. First we use HDF5 to extract the data from a very big file so we can look at the parameters we are interested in obtained via parameter estimation and nested sampling. Now we want to analyse the 2PN term ϕ_4 from Eq. (51) by placing upper bounds and lower bounds on K where the values of $\delta\phi_4$ are extracted from the data. We do this by taking an integral over the graph and let it end on 0.05 and 0.95 so we get an 90% credible interval as in [6] which means 90% of the distribution of K lies in between the bounds.

90% credible interval		
event name	lower bound K	upper bound K
GW170608	-0.616999	1.016000
GW151226	-1.272000	0.943999

From this table we can directly see that GW170608 has the best bounds on K. Now we want to compare this to the bounds set by the EHT on the M87 black hole for the 2PN term. In the article of Psaltis et al [24] the expression for the shadow radius (Eq. (9) from chapter 2) is written as:

$$r_{sh,JP} = 3\sqrt{3}\left[1 + \frac{1}{27}\alpha_{13} - \frac{1}{486}\alpha_{13}^2 + \mathcal{O}(\alpha_{13}^3)\right] \tag{105}$$

The results for α_{13} are given in the next figure

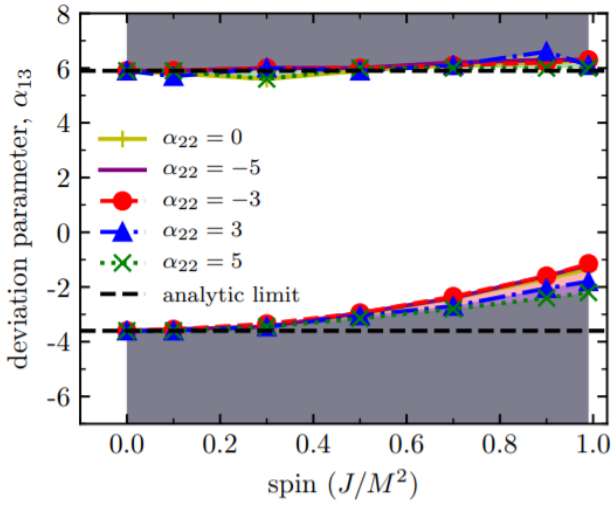

Figure 9: Bound on the deviation parameter α_{13} of the JP metric where different values of α_{22} represents some other parameter we are not interested in. Here the deviation (of α_{31}) is given as a function of the spin.[24]

If we don't take into account the spin and require that the shadow size is consistent to within 17% with the 2017 EHT measurement of the picture made of M87 we get a bound on the deviation parameter α_{13} of $-3.6 < \alpha_{13} < 5.9$ [24]. From Eq. (105) and Eq. (9) we see that $\frac{1}{3}\alpha_{13} = K$. Translated to K the bounds for the 2PN parameter coming from EHT are then: $-1.2 < K < 1.966667$. Comparing this to the best gravitational wave event GW170608, they both yield quite the same accuracy. We can read from the plot that GW170608 has a total bound of around $-1.2 < K < 2$. The event GW151226 gives a total bound of around $-2.5 < K < 2$. Here the total bound means that all the values say 100% lay between this bound. Now in our code we calculated the 90% credible interval for some arbitrary reason. The results of Psaltis et al[24] gives us the 100% interval and besides reading of from the plot we could also change the code and calculate the 100% interval for the GW events. If we integrate from say 0.001 to 0.999 instead of 0.05 to 0.95 we get for GW170608 a bound of $-1.662999 < K < 1.828999$ which is fairly close to the EHT measurements, but especially the lower bound differs somewhat. Furthermore if we increase the credible interval we see that our distribution for K in the GW events is not a perfect symmetrical Gaussian because the lower bound tend to go farther away from the median.

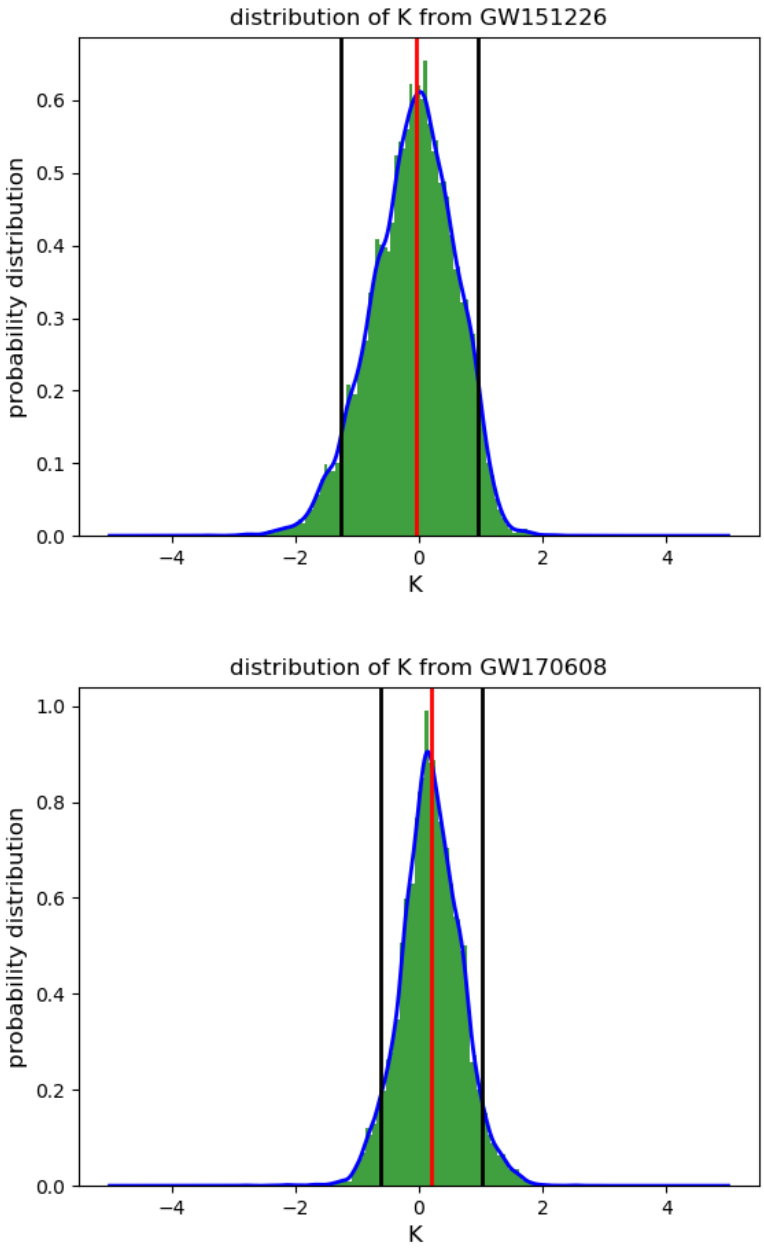

Figure 10: Plots of the deviations K form the 2PN therm with upperbounds and lowerbounds in black and the median in red

7 Discussion

There are some assumptions made in this thesis that may need some further discussion. First of all, for the gravitational wave energy Eq. (75) we assumed that it just follows from GR, because it's the most convenient option. But in this thesis we are testing GR so:

- hypothetically GR is wrong and with that the theoretical obtained expression for $\dot{E}_{gw}$ could be different. But because of the lack of fundamental theory we have to settle with Eq. (75)
- Alternatively GR is perfectly fine and deviations from the analytical results of GR with respect to the 2PN term are the consequence of the existence of exotic objects such as boson stars which we mistaken for black holes.

We also made the assumption that our parameter K is small in section 5.1, this resulted in a fairly simple expression for the radius $r(\omega)$ and hence the energy $E(\omega)$. However, from the measurements of K we know it can be bigger than one and thus K^2 and higher orders of K shouldn't be neglected. For a more robust test of GR we could consider taking higher order terms into account.

Furthermore, we know that black holes have spin as could be seen in section 6.1 of parameter estimation. We assumed that there is no spin for the black holes. In figure (8) we see that for the deviation parameter obtained from the EHT picture that spin does play a role in determining the bound on K. However, from [30] we see that the ϕ_4 term has an extra $-\sigma$ in between the brackets. This sigma encodes the spin related effects and small compared to the other terms. That way we can neglect the spin.

Besides these assumptions there are also limitation in to what extend in the process of inspiral we can make good measurements. One may wonder why we get more or less the same results for the bound on K with gravitational waves as with optical measurements and not better. This is meanly due to the fact that beyond the merger phase of inspiral, detection of gravitational waves become increasingly difficult because of large redshifts in the GW's coming from the inspiraling binaries. We speculate that this is because for gravitational waves, the "resolution" with which a binary black hole system is being probed is essentially set by the sizes of the photon spheres of the individual black holes, since contributions to the gravitational wave signal coming from much closer to a black hole get gravitationally redshifted out of our detectors' sensitive band [14]. However, this question deserves more scrutiny; this we leave for future work.

8 Conclusions and future directions

In this thesis we explored the possibility for testing GR with the help of gravitational waves. We have done so by expanding Newton's universal law of gravity by a $1/r^3$ term which led to a 2PN deviation parameter K on which we have set bounds on using data from the events GW170608 and GW151226. These events have been detected by Advanced LIGO and Advanced Virgo and from that data we got bounds for K. The same had been done by the use of the picture of black hole M87 taken with the EHT. We can say that our data from the GW detections gives bounds on K comparable with those set by the measurement of the EHT picture of M87. For the near future, we can make improvements of our analysis that are current within reach such as taken into account higher order's of K in the expression for the energy $E(\omega)$ and take spin into account. For the far future we can use the so called third generation detectors (Advanced LIGO/Virgo are 2nd generation) to get more GW signals and more important signals from GW's coming from binary inspiral stages which are currently undetectable.
Far more improvements have to be made but we can say gravitational wave physics is very promising for the future. It has been only 5 years after the first GW detection and we are now on the point that we are able to do useful research on fundamental physics. That is very hopeful and it already opened a new gateway to the universe.

References

[1] *Data release for testing gr with gwtc-1 events*. `https://dcc.ligo.org/LIGO-P1900087/public`. Accessed: 2021-15-6.

[2] *Gravitational wave data analysis: Ii. model selection and parameter estimation*. `https://solisservices-my.sharepoint.com/personal/c_f_f_vandenbroeck_uu_nl/Documents/Attachments/Cambridge_II_v3.pdf`. Accessed: 2-06-2021.

[3] *Infinite visions were hiding in the first black hole image's rings*. `https://www.nytimes.com/2020/03/28/science/black-hole-rings.html`. Accessed: 2021-10-6.

[4] *Ligo detects second black-hole merger*. `https://physicsworld.com/a/ligo-detects-second-black-hole-merger/`. Accessed: 2021-16-6.

[5] *Ligo timeline*. `https://www.ligo.caltech.edu/page/timeline`. Accessed: 19-05-2021.

[6] B. Abbott, R. Abbott, T. Abbott, S. Abraham, F. Acernese, K. Ackley, C. Adams, R. Adhikari, V. Adya, C. Affeldt, and et al., *Tests of general relativity with the binary black hole signals from the ligo-virgo catalog gwtc-1*, Physical Review D, 100 (2019).

[7] B. P. Abbott, *Gw170814: A three-detector observation of gravitational waves from a binary black hole coalescence*, Phys. Rev. Lett., 119 (2017), p. 141101.

[8] B. P. Abbott et al., *Observation of Gravitational Waves from a Binary Black Hole Merger*, Phys. Rev. Lett., 116 (2016), p. 061102.

[9] K. Akiyama and K. Bouman, *First m87 event horizon telescope results. iv. imaging the central supermassive black hole*, Astrophysical Journal Letters, 875 (2019).

[10] K. Akiyama et al., *First M87 Event Horizon Telescope Results. I. The Shadow of the Supermassive Black Hole*, Astrophys. J. Lett., 875 (2019), p. L1.

[11] P. Amaro-Seoane et al., *Laser Interferometer Space Antenna*, (2017).

[12] K. Arun, B. R. Iyer, B. Sathyaprakash, and P. A. Sundararajan, *Parameter estimation of inspiralling compact binaries using 3.5 post-Newtonian gravitational wave phasing: The Non-spinning case*, Phys. Rev. D, 71 (2005), p. 084008.

[13] T. W. Baumgarte and S. L. Shapiro, *Binary black hole mergers*, Phys. Today, 64N10 (2011), pp. 32–37.

[14] E. Berti, V. Cardoso, and C. M. Will, *On gravitational-wave spectroscopy of massive black holes with the space interferometer LISA*, Phys. Rev. D, 73 (2006), p. 064030.

[15] T. Damour, B. R. Iyer, and B. S. Sathyaprakash, *A Comparison of search templates for gravitational waves from binary inspiral - 3.5PN update*, Phys. Rev. D, 66 (2002), p. 027502.

[16] T. Damour, B. R. Iyer, and B. S. Sathyaprakash, *Comparison of search templates for gravitational waves from binary inspiral: 3.5PN update*, , 66 (2002), p. 027502.

[17] A. Einstein, *The Foundation of the General Theory of Relativity*, Annalen Phys., 49 (1916), pp. 769–822.

[18] K. Gebhardt, J. Adams, D. Richstone, and et al., *Lecture notes on gravitational waves*, Apj, 279 (2011), pp. –.

[19] C. Herdeiro, J. Kunz, I. Perapechka, E. Radu, and Y. Shnir, *Multipolar boson stars: Macroscopic bose-einstein condensates akin to hydrogen orbitals*, Physics Letters B, 812 (2021), p. 136027.

[20] R. A. Hulse and J. H. Taylor, *Discovery of a pulsar in a binary system*, Astrophys. J, 195 (2011), pp. –.

[21] M. Maggiore, *Gravitational Waves. Vol. 1: Theory and Experiments*, Oxford Master Series in Physics, Oxford University Press, 2007.

[22] D. Morin, *Introduction to Classical Mechanics: With Problems and Solutions*, Cambridge University Press, 2008.

[23] V. Perlick and O. Y. Tsupko, *Calculating black hole shadows: review of analytical studies*, (2021).

[24] D. Psaltis et al., *Gravitational Test Beyond the First Post-Newtonian Order with the Shadow of the M87 Black Hole*, Phys. Rev. Lett., 125 (2020), p. 141104.

[25] M. Punturo et al., *The Einstein Telescope: A third-generation gravitational wave observatory*, Class. Quant. Grav., 27 (2010), p. 194002.

[26] B. Sathyaprakash and B. F. Schutz, *Physics, astrophysics and cosmology with gravitational waves*, Living Reviews in Relativity, 12 (2009), pp. –.

[27] J. Skilling, *Nested sampling for general Bayesian computation*, Bayesian Analysis, 1 (2006), pp. 833–859.

[28] N. A. Tikhonov, *The distance to the giant elliptical galaxy m87 and the size of its stellar subsystem*, Astrophysical Bulletin, 74 (2019), pp. 257–269.

[29] S. L. Tiscione, *Ligo*.

[30] C. Van Den Broeck and A. S. Sengupta, *Binary black hole spectroscopy*, Class. Quant. Grav., 24 (2007), pp. 1089–1114.

[31] J. Veitch and A. Vecchio, *Bayesian coherent analysis of in-spiral gravitational wave signals with a detector network*, Phys. Rev. D, 81 (2010), p. 062003.